

# Laser-induced thermal lens effect: a new theoretical model

S. J. Sheldon, L. V. Knight, and J. M. Thorne

A theoretical model for the laser-induced thermal lens effect in weakly absorbing media is derived. The model predicts the intensity variation in the far field of the laser beam in the presence of the lensing medium and takes into account the aberrant nature of the thermal lens. Some experimental results which support the validity of this approach are presented.

## I. Introduction

Thermal lensing or thermal blooming occurs as energy absorbed from a Gaussian beam produces local heating of an absorbing medium about the beam axis. A radially dependent temperature distribution is created which in turn produces a refractive-index change by the factor  $dn/dT$ , the change of refractive index with temperature. This turns the medium into a lens for the beam. The development of this thermal lens occurs over the brief time it takes the beam to reach thermal equilibrium with the medium. In most liquid media the refractive-index changes because of a decrease in density with increasing temperature. In such cases  $dn/dT$  is negative, and the thermal lens is a negative or diverging lens. As the lens develops there is a spreading of the beam and a drop in its intensity. By measuring the magnitude and time dependence of the intensity change with a small aperture photodetector placed at the beam center beyond a cell containing the sample medium, the thermo-optic properties of the sample can be studied.

The thermal lens effect was first reported by Gordon *et al.* in 1964,<sup>1</sup> and an expression for the focal length of the lensing medium was derived. Later, Hu and Whinnery<sup>2,3</sup> derived an expression for the intensity variation in the far field of a Gaussian beam which passes through a thermal lensing medium. These

models are based on an approximation in which the lens has a parabolic refractive-index distribution so that it can be treated as a perfect thin lens—one having no aberrations. The parabolic model describes the general behavior of the thermal lens quite well but is not quantitatively accurate. A more accurate model can be derived by taking into account the true aberrant nature of the thermal lens.

## II. Theory

The components of the thermal lensing experiment are arranged as shown in Fig. 1. The laser will operate in the TEM<sub>00</sub> mode giving a Gaussian intensity distribution. The beam passes through a converging lens so that it is focused down to a waist. The location of the waist is taken as the origin along the  $z$  axis. A sample cell of length  $l$  is located at  $z_1$ , and a photodetector is centered in the beam at the position  $z_1 + z_2$ . Its aperture is made small compared with the beam diameter at this location. The lensing effect in the cell causes a slight intensity drop in the beam which is sensed by the detector.

The absorbance  $b$  and the beam divergence angle are small allowing the beam power  $P$  and the beam radius  $\omega$  to be taken as constants within the cell. The length and transverse dimensions of the cell are large compared with the diameter of the beam so that the medium can be considered as infinite in the radial coordinate, heat conduction through the ends can be neglected, and thus the temperature variation can be taken as purely radial.

In the derivations the following symbols will be used:

$b$	absorbance, $\text{cm}^{-1}$ ;
$\rho$	density, $\text{g cm}^{-3}$ ;
$I$	beam intensity, $\text{cal sec}^{-1} \text{cm}^{-2}$ ;
$l$	cell length, $\text{cm}$ ;
$P$	beam power, $\text{W}$ ;

The authors are with Brigham Young University, Department of Physics & Astronomy, Provo, Utah 84602.

Received 23 November 1982.

0003-6935/82/091663-09\$01.00/0.

© 1982 Optical Society of America.

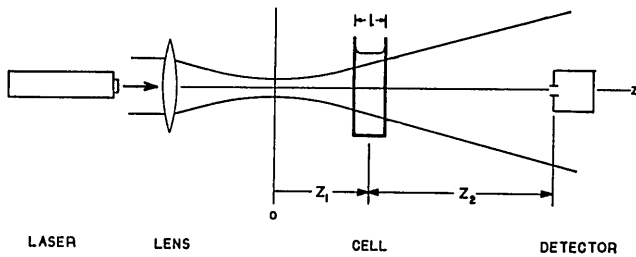


Fig. 1. Components of the thermal lensing experiment.

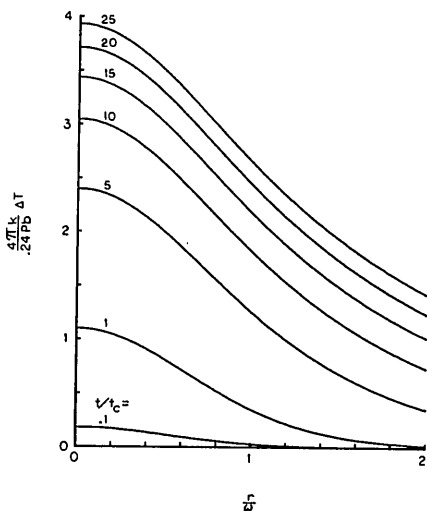


Fig. 2. Temperature distribution in the thermal lens at various times.

- $z$  position along beam axis, cm;
- $r$  radius with respect to beam axis, cm;
- $n$  refractive index;
- $c$  specific heat,  $\text{cal g}^{-1} \text{K}^{-1}$ ;
- $\omega$  beam radius, cm;
- $\Delta T$  temperature change, K;
- $k$  thermal conductivity,  $\text{cal sec}^{-1} \text{cm}^{-1} \text{K}^{-1}$ ;
- $\kappa$  thermal diffusivity,  $k/c\rho$ ,  $\text{cm}^2 \text{sec}^{-1}$ ; and
- $\lambda$  wavelength, cm

An expression for the temperature change in the sample as a function of radius and time  $\Delta T(r,t)$  can be obtained by solving the nonsteady state heat equation<sup>4</sup> appropriate for the problem:

$$c\rho \frac{\partial}{\partial t} [\Delta T(r,t)] = \dot{q}(r) + k\nabla^2[\Delta T(r,t)]; \quad (1)$$

$$r < \infty;$$

$$\Delta T(r,0) = 0.$$

The quantity  $\dot{q}(r)$ , the source term, is the energy flow into a unit volume per unit time at a distance  $r$  from the axis. The intensity change in the laser light as it passes through the absorbing medium can be written as

$$\Delta I(r) = I_0(r) - I(r) \simeq I_0(r)bl, \quad (2)$$

where  $I_0(r)$  is the beam intensity entering the sample at  $r$ ,  $I(r)$  is the exiting beam intensity, and  $b$  is small. Therefore,

$$\dot{q}(r) = \frac{\Delta I(r)}{l} = I_0(r)b. \quad (3)$$

For a Gaussian beam the input intensity  $I_0(r)$  is<sup>5</sup>

$$I_0(r) = \frac{2(0.24P)}{\pi\omega^2} \exp(-2r^2/\omega^2). \quad (4)$$

By combining Eqs. (3) and (4) the source term becomes

$$\dot{q}(r) = \frac{2(0.24P)b}{\pi\omega^2} \exp(-2r^2/\omega^2). \quad (5)$$

Whinnery<sup>2</sup> showed that the solution to Eq. (1) is

$$\Delta T(r,t) = \frac{2(0.24P)b}{\pi c\rho\omega^2} \int_0^t \left( \frac{1}{1+2t'/t_c} \right) \times \exp\left( \frac{-2r^2/\omega^2}{1+2t'/t_c} \right) dt', \quad (6)$$

where

$$t_c = \frac{\omega^2 c\rho}{4k} = \frac{\omega^2}{4\kappa}. \quad (7)$$

This integral, the exponential integral, can be written in its series form as<sup>6</sup>

$$\Delta T(r,t) = \frac{0.24Pb}{4\pi k} \left\{ \ln\left(1 + \frac{2t}{t_c}\right) + \sum_{m=1}^{\infty} \frac{(-2r^2/\omega^2)^m}{mm!} \times \left[ 1 - \frac{1}{(1+2t/t_c)^m} \right] \right\}. \quad (8)$$

Equations (6) and (8) are the desired expressions for the temperature change in the sample. The quantity  $t_c$  defined by Eq. (7) is the time constant and is the characteristic buildup time of the thermal lens. The curves of Fig. 2 are computer generated plots of Eq. (8). They show the predicted time evolution of the temperature distribution. They are considerably different from those arising from the parabolic approximation in which only the first term in the series of Eq. (8) is used.

The refractive index as a function of radius and time can be obtained by substituting Eq. (6) or (8) for  $\Delta T(r,t)$  into the expression

$$n(r,t) = n_0 - \frac{dn}{dT} \Delta T(r,t), \quad (9)$$

where  $n_0$  is the refractive index at the initial temperature. Equation (9) assumes a decrease in refractive index with increased temperature, and  $dn/dT$  is an absolute value.

The next step is to determine what effect this refractive-index distribution has on the beam intensity for points on the axis beyond the cell. The approach is based on the diffraction theory of aberrations and begins with a statement of the Huygens principle: The complex phase amplitude of a wave at a point on an output plane is the result of a superposition of the Huygens wavelets emanating from all points on an input plane. This is written as<sup>5</sup>

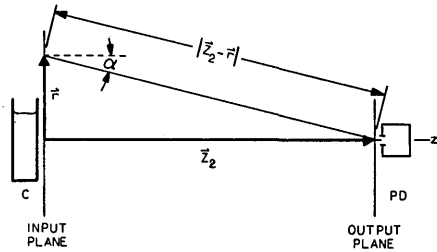


Fig. 3. Symbols used in the diffraction integral.

$$\begin{aligned} \bar{U}_{bc}(t) = & \frac{i}{\lambda} \int_0^\infty \int_0^{2\pi} \bar{U}_i(r,t) \left( \frac{1 + \cos\alpha}{2} \right) \\ & \times \frac{\exp[-i(2\pi/\lambda)|z_2 - \mathbf{r}|]}{|z_2 - \mathbf{r}|} r dr d\theta, \end{aligned} \quad (10)$$

the diffraction integral. Figure 3 indicates the meanings of the symbols.  $\bar{U}_i(r,t)$  is the complex phase and amplitude of the waves at the input plane or where they exit the sample cell. The second quantity in the integrand is the inclination factor, and the third quantity is the phase and attenuation of the wave after traversing a distance  $|z_2 - \mathbf{r}|$ .  $\bar{U}_{bc}(t)$  is the complex phase and amplitude of waves on the axis or the beam center at the output plane where the detector is located.

At this point some simplifying approximations are made on Eq. (10). Since the transverse dimensions of the beam are  $\ll z_2$ ,

$$|z_2 - \mathbf{r}| \approx z_2, \quad (11)$$

$$\frac{1 + \cos\alpha}{2} \approx 1, \quad (12)$$

and in the exponential

$$\frac{2\pi}{\lambda} |z_2 - \mathbf{r}| \approx \frac{2\pi}{\lambda} \left( z_2 + \frac{r^2}{2z_2} \right). \quad (13)$$

With these the integral becomes

$$\bar{U}_{bc}(t) = A \int_0^\infty \int_0^{2\pi} \bar{U}_i(r,t) \exp\left(-i \frac{\pi r^2}{\lambda z_2}\right) r dr d\theta, \quad (14)$$

where all constants are represented by  $A$ .

An expression for  $\bar{U}_i(r,t)$  is found by first ignoring the effects of the lensing medium and assuming the beam to be composed of spherical waves with radius of curvature  $R$  and a Gaussian amplitude distribution. The amplitude factor is

$$|\bar{U}_i| = B \exp(-r^2/\omega^2), \quad (15)$$

where  $B$  is a constant and  $\omega$  is the beam radius. The phase at points on the input plane is

$$\frac{2\pi}{\lambda} L = \frac{2\pi}{\lambda} (R^2 + r^2)^{1/2}, \quad (16)$$

$$\approx \frac{2\pi}{\lambda} (R + r^2/2R), \quad (17)$$

as can be seen by studying Fig. 4(a). The approximation is valid in this case since the beam is confined to a narrow region about the axis so that  $R \gg r$ . The rela-

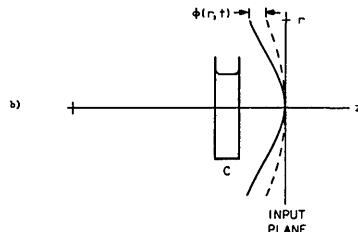
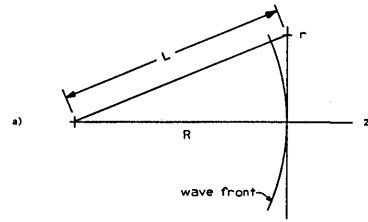


Fig. 4. Phase distribution at the input plane: (a) with the lensing medium absent; and (b) with the lensing medium present.

tive phase distribution or phase lag is therefore

$$(\pi r^2)/(\lambda R). \quad (18)$$

Following Born and Wolf<sup>7</sup> the effect of the lensing medium is considered as an aberration. It is included as a small perturbation in the form of an additional phase lag to the phase term of the spherical wave, expression (18). The spherical waves emerge from the cell at the input plane slightly distorted as shown in Fig. 4(b). An expression for this additional phase lag is found by considering the problem from the point of view of the optical path length in the medium. Initially, the optical path length is

$$\Phi_0 = n_0 l. \quad (19)$$

The optical path length variation about the axis is written as

$$\Phi(r,t) = l[n(r,t) - n(0,t)]. \quad (20)$$

Substituting Eq. (9) into this for  $n$  and multiplying both sides by  $2\pi/\lambda$  give

$$\frac{2\pi}{\lambda} \Phi(r,t) = \frac{2\pi}{\lambda} \frac{dn}{dT} l[\Delta T(0,t) - \Delta T(r,t)], \quad (21)$$

which is the desired expression for the additional phase lag. With (15), (18), and (21) the expression

$$\bar{U}_i(r,t) = B \exp(-r^2/\omega^2) \exp(-i(\pi/\lambda)(r^2/R + 2\Phi)) \quad (22)$$

is obtained for the complex phase and amplitude at the input plane. Substituting this expression for  $\bar{U}_i$  into Eq. (14), making the change of variable  $u = r^2/\omega^2$ , and carrying out the integration over  $\theta$  give

$$\begin{aligned} \bar{U}_{bc}(t) = & C \int_0^\infty \exp - \left\{ u + i \left[ \frac{2\pi}{\lambda} \Phi(u,t) \right. \right. \\ & \left. \left. + \frac{\pi\omega^2}{\lambda} \left( \frac{1}{R} + \frac{1}{z_2} \right) u \right] \right\} du \end{aligned} \quad (23)$$

for the diffraction integral.

The following substitutions can be made for  $R$  and  $\omega$  in the phase factor<sup>8</sup>

$$\omega(z_1) = \omega_0 [1 + (z_1/z_c)^2]^{1/2}, \quad (24)$$

$$R(z_1) = \frac{1}{z_1} (z_1^2 + z_c^2), \quad (25)$$

where

$$z_c = \frac{\pi \omega_0^2}{\lambda}. \quad (26)$$

$z_c$  is called the confocal parameter of the Gaussian beam, and  $\omega_0$  is the spot size or the beam radius at the waist ( $z = 0$ ). With these the third term in the integrand becomes

$$i \left[ \frac{z_1}{z_c} + \frac{z_1}{z_2} \left( \frac{z_1}{z_c} + \frac{z_c}{z_1} \right) \right] u. \quad (27)$$

If the detector is placed in the far field so that  $z_2 \gg z_1$  all terms in (27) involving  $z_2$  can be dropped.  $z_1$  and  $z_c$  are generally of the same order.

Another approximation will be made at this point. It is

$$\exp[-i(2\pi/\lambda)\Phi] \approx 1 - i \frac{2\pi}{\lambda} \Phi, \quad (28)$$

where it is assumed that  $(2\pi/\lambda)\Phi \ll 1$ . This condition is easily met in thermal lensing experiments. With these modifications the diffraction integral becomes

$$\bar{U}_{bc}(t) = C \int_0^\infty \left( 1 - i \frac{2\pi}{\lambda} \Phi \right) \exp[-(1 + i\zeta)u] du, \quad (29)$$

where  $\zeta = z_1/z_c$ .

Substituting Eq. (6) into Eq. (21) gives

$$\frac{2\pi}{\lambda} \Phi(u, t) = \frac{\theta}{t_c} \int_0^t \tau [1 - \exp(-2\tau u)] dt' \quad (30)$$

for the additional phase lag, where

$$\theta = \frac{0.24Pl b}{\lambda} \frac{dn}{k dT}, \quad (31)$$

$$\tau(t') = \frac{1}{1 + 2t'/t_c}. \quad (32)$$

As suggested by Eq. (30), approximation (28) is good when  $\theta$  is sufficiently small. In most thermal lensing experiments the parameters involved in expression (31) are so that  $\theta$  is of the order of 0.1 or less.

With the substitution of Eq. (30) the diffraction integral becomes finally

$$\bar{U}_{bc}(t) = C \int_0^\infty \left\{ 1 - i \frac{\theta}{t_c} \int_0^t \tau [1 - \exp(-2\tau u)] dt' \right\} \times \exp[-(1 + i\zeta)u] du. \quad (33)$$

The integration over  $u$  is carried out first followed by  $t'$ .

In finding the intensity variation  $I_{bc}(t) = |\bar{U}_{bc}(t)|^2$  all terms of order  $\theta^2$  are neglected, and a convenient form for the equations is the fractional intensity change,  $[I(t) - I(\infty)]/I(\infty)$ . The result is

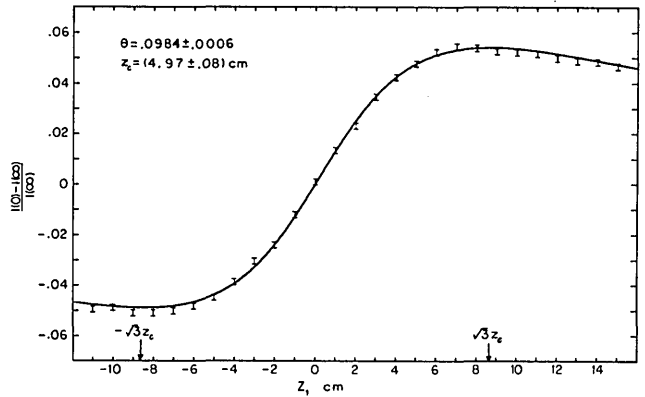


Fig. 5. Thermal lens position data and best fit curve.

$$\frac{I(t) - I(\infty)}{I(\infty)} = \frac{1 - \theta \tan^{-1} \left[ \frac{2\zeta}{3 + \zeta^2 + (9 + \zeta^2)(t_c/2t)} \right]}{1 - \theta \tan^{-1} \left( \frac{2\zeta}{3 + \zeta^2} \right)} - 1. \quad (34)$$

The total fractional intensity change found by setting  $t = 0$  is

$$\frac{I(0) - I(\infty)}{I(\infty)} = \frac{1}{1 - \theta \tan^{-1} \left( \frac{2\zeta}{3 + \zeta^2} \right)} - 1. \quad (35)$$

Through the dependence of  $t_c$  on  $\omega(z_1)$  [see Eq. (7)] and the dependence of  $[I(0) - I(\infty)]/I(\infty)$  on  $z_1$ , both the magnitude and time dependence of the thermal lens effect are sensitive to the location of the cell  $z_1$  with respect to the waist. Setting the derivative of Eq. (35) with respect to  $\zeta$  equal to zero leads to the prediction that the effect is optimized when  $\zeta = \pm\sqrt{3}$  or the cell is located at  $\sqrt{3}$  confocal distances in front of or behind the waist. This is shown in Fig. 5, which is a fit of Eq. (35) to some measured values of  $[I(0) - I(\infty)]/I(\infty)$  vs  $z_1$ . Note that when the cell is at the waist no lens effect is predicted. When it is behind the waist at negative values of  $z_1$  the effect is inverted.

If the cell is located at  $z_1 = \sqrt{3}z_c$ , expression (34), the expression for the fractional intensity change at the beam center in the far field becomes

$$\frac{I(t) - I(\infty)}{I(\infty)} = \frac{1 - \theta \tan^{-1} \left( \frac{0.577}{1 + t_c/t} \right)}{1 - \theta(0.524)} - 1. \quad (36)$$

### III. Experiment

The experiment was designed to test Eqs. (35) and (36), the thermal lens equations, when all parameters of both the sample and beam were known. The three parameters of interest in the equations are  $\theta$  where

$$\theta = \frac{0.24Pl b}{\lambda} \frac{dn}{k dT}, \quad (31)$$

the time constant  $t_c$  where

$$t_c = \frac{\omega^2 c \rho}{4k} = \frac{\omega^2}{4\kappa}, \quad (7)$$

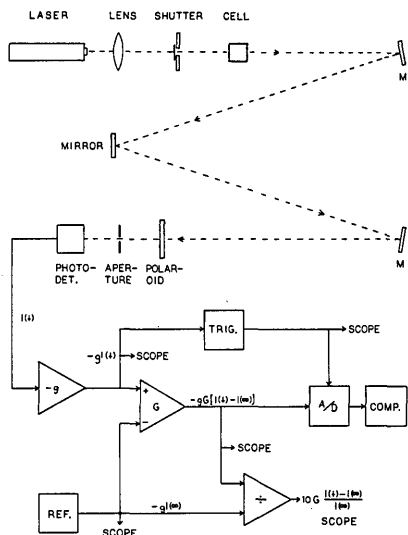


Fig. 6. Optical layout and electronics block diagram.

and the confocal parameter of the beam  $z_c$  where

$$z_c = \frac{\pi \omega_0^2}{\lambda} \quad (26)$$

The thermo-optic constants  $b$ ,  $dn/dT$ ,  $k$ ,  $c$ , and  $\rho$  are variables depending on the sample; and the parameters  $P$ ,  $l$ ,  $\lambda$ ,  $z_c$ , and  $\omega$  are constants of the system. When Eqs. (35) and (36) are fitted to data, values of  $\theta$ ,  $t_c$ , and  $z_c$  are obtained from which the system constants are calculated. These are compared with their expected values.

The optical layout and electronics block diagram is shown in Fig. 6. The laser is a He-Ne laser operating at 6328 Å in the TEM<sub>00</sub> mode with an output power of 9.5 mW as measured by a Spectra-Physics model 4018, 6328-Å power meter. The beam passes through a 20.7-cm focal length lens first, then through the sample cell which is a 1-cm path length quartz absorption cell. The shutter, a Uniblitz model 225L, is mounted beyond the lens at the beam waist. The beam is folded back three times by mirrors to make a separation between the cell and the photodetector of ~340 cm. The third mirror has adjustment screws so that its tilt angle can be varied allowing the beam to be centered on the detector. A Polaroid plate is mounted in front of the detector which can be rotated to make coarse adjustments on the beam intensity. The aperture, a 0.1524-cm (0.060-in.) hole drilled in a piece of shim, brass is built into the photodetector assembly. The photodetector consists of an MRD 500 photodiode and a one-transistor current amplifier. The amplified photocurrent is sent to a current-to-voltage amplifier with variable gain whose output is proportional to  $I_{bc}(t)$ . Also in the circuit is a reference voltage source set to 5 V. The gain of the signal amplifier  $g$  is set so that  $I_{bc}(\infty)$  is approximately equal to this 5-V reference level. When signal and reference voltages are combined in the summing amplifier, an output proportional to  $I(t) - I(\infty)$  is obtained which is sent to the analog divider.

Table I. Thermo-optic Constants of the Four Samples

Sample	$c$	$\rho$	$k$ $\times 10^4$	$\kappa = k/c\rho$ $\times 10^4$	$-(dn/dT)$ $\times 10^4$
Water	1.0	1.0	14.2	14.2	0.8
Methanol	0.609	0.79	4.83	10.04	3.9
Ethanol	0.586	0.791	4.00	8.63	3.9
Carbon tetrachloride	0.206	1.59	2.46	7.51	5.8

Source Refs. 1, 9, and 10.

The signal produced by the analog divider is used only for rough monitoring on the oscilloscope. The signal from the summing amplifier is also sent to an analog-to-digital converter (ADC) programmed to sample at set time intervals. These data in the form  $I(t) - 5$  are sent to a computer for manipulation to obtain values of  $[I(t) - I(\infty)]/I(\infty)$ .

An experiment begins when the shutter opens. The leading edge of the signal fires the trigger circuit which in turn starts both the sampling sequence of the ADC and the horizontal sweep of the oscilloscope. The shutter is held open long enough for the signal to reach a steady state or for the thermal lens to become fully developed. The last sample taken just before the shutter closes is used as  $I(\infty) - 5$  to calculate the exact value of  $[I(t) - I(\infty)]/I(\infty)$  for each data sample. These values are stored in an array. With the closing of the shutter one experiment is completed. Several experiments are performed in a sample run so that several sets of  $[I(t) - I(\infty)]/I(\infty)$  values are obtained. These are then averaged by the computer.

Four test samples were chosen which had known thermo-optic constants. They were chosen to have a wide range of evenly spaced thermal diffusivities, the choices being limited by the availability of literature data. They were carbon tetrachloride, methanol, ethanol, and water. The constants are listed in Table I. By adding blue dyes the absorbances were adjusted to any desired value.

Before any data could be taken it was necessary to locate the beam waist and measure the beam radius  $\omega_0$  at the waist. A 25- $\mu$ m pinhole was placed over the input of the 4018 power meter, centered in the beam, and moved along the beam axis. The power was plotted as a function of position. The place where it had its maximum was taken as the location of the waist. The beam radius  $\omega_0$  was found next. The pinhole-4018 assembly was moved along the beam axis, and the power was noted at several positions relative to the waist. The beam radii squared  $\omega^2(z)$  at each location were calculated from the power readings and the integral of intensity over the area of the pinhole normalized to the total power of the beam. A least squares fit of a straight line to the  $\omega^2$  vs  $z^2$  data was made [see Eq. (24)] giving an intercept of  $\omega_0^2 = (9.54 \pm 1.93) \times 10^{-5}$  cm<sup>2</sup> from which a value of  $z_c = (4.74 \pm 0.96)$  cm was calculated. The rather large uncertainties of these values resulted from an assumed tolerance on the pinhole of  $\pm 1$   $\mu$ m. With the parameters  $\omega_0$  and  $\lambda$  and the waist location, the beam was completely specified.

A sample of methanol and methylene blue was prepared to give a  $\theta$  of  $\sim 0.1$ . This was placed in the beam, and  $[I(0) - I(\infty)]/I(\infty)$  readings were taken every centimeter from  $-11$  to  $15$  cm relative to the waist. Twenty experiments were performed at each location and the data averaged. Stored in the computer was a curve fitting program which calculated a least squares fit of Eq. (35) to the data, adjusting the sigmas of the data points to give a reduced chi-square of 1. The optimized parameters of the fit were  $\theta = 0.0984 \pm 0.0006$  and  $z_c = (4.97 \pm 0.08)$  cm. The data and best fit curve are plotted in Fig. 5. The  $z_c$  value obtained from the fit was in good agreement with the expected value obtained by the pinhole method.

Using the value of  $z_c$  obtained from the fit of Eq. (35) to the position data, the optimum location of the cell was determined. With the cell in this position, the  $\theta$  and  $t_c$  dependences can be studied. For measurements of the  $\theta$  dependence, solutions of water with bromothymol blue and 1 gram/liter  $K_2HPO_4$  were used. The absorbances  $b$  in these samples represent the sum of the solvent absorbances  $b_s$  and the dye absorbances  $b_d$ , or

$$b = b_s + b_d. \quad (37)$$

A starting solution was prepared which had a  $b_d$  of  $\sim 0.5$   $\text{cm}^{-1}$  as measured in a Beckman DU spectrophotometer using the  $H_2O-K_2HPO_4$  solvent as a reference. Dilutions were made with this starting solution to give various values of  $b_d$ . Each sample was placed in the thermal lensing apparatus and given about five runs of thirty experiments each. For each experiment the ADC was programmed to sample at a rate of about fifty samples per ten time constants. Several times during a run the lateral position of the cell was shifted slightly to average out the effects of surface irregularities on the cell faces, and the beam was recentered on the photodetector in case it had drifted. This seemed to be critical in obtaining reproducible values for  $t_c$ .

A least squares fit of Eq. (36) was made to the first fifty data values or out to about ten time constants which yielded optimized values of  $\theta$  and  $t_c$ . Figure 7 shows the data and best fit curve for one of these samples.

There exists a linear relationship between  $\theta$  and  $b_d$  which, using Eqs. (31) and (37), can be expressed as

$$\theta = \left( \frac{0.24Pl}{\lambda} \right) \frac{b_d}{k} \frac{dn}{dT} + \frac{0.24Plb_s}{k\lambda} \frac{dn}{dT}, \quad (38)$$

where  $\theta$  is the dependent variable and  $b_d/k \cdot (dn/dT)$  is the independent variable. The quantity in parentheses is the slope and the desired system constant. The second term is the intercept and is related to the absorbance of the pure solvent  $b_s$ . A least squares fit of Eq. (38) to the  $\theta$  vs  $b_d/k \cdot (dn/dT)$  data gave  $0.24Pl/\lambda = (33.4 \pm 0.4)$   $\text{cal sec}^{-1}$ . This was in good agreement with the expected value of 31.7 obtained by measuring  $P$  with the 4018 power meter allowing for the reflection loss at the front surface of the cell.

The data are plotted with the best fit straight line in Fig. 8. The fit was made to only the first six points

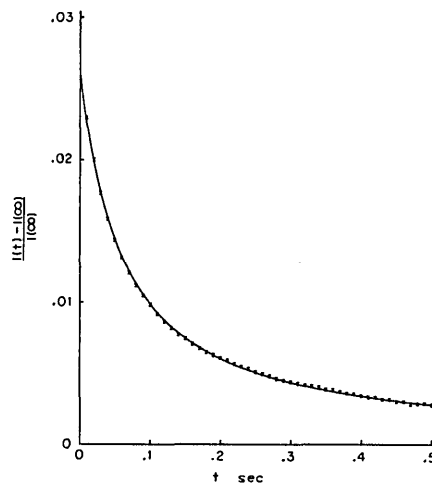


Fig. 7.  $[I(t) - I(\infty)]/I(\infty)$  vs  $t$  data and best fit curve for a sample of water-1 g/l  $K_2HPO_4$  and bromothymol blue.

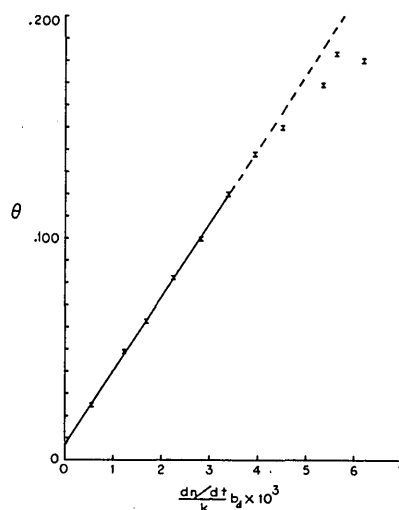


Fig. 8.  $\theta$  vs  $(b_d/k)(dn/dT)$  data and best fit line for samples of water-1 g/l  $K_2HPO_4$  and bromothymol blue.

which showed a clearly linear behavior. The line was extrapolated up through the remainder of the points to show that a deviation from linearity occurs when, presumably,  $\theta$  was too large or when approximation (28) is not good. A weighted average of the  $t_c$  values obtained from the first six samples was taken and used in the next part of the experiment.

Measurements were next taken with the thermal lensing apparatus to obtain values of  $t_c$  for carbon tetrachloride with Sudan black dye and for methanol and ethanol both with methylene blue dye. The thermal lensing time dependence of a sample is related only to its thermal diffusivity  $\kappa = k/c\rho$ ; therefore it was not necessary to know absorbances here as it was with the water samples. The dyes were added only to make the absorbances large enough to produce easily measurable signals.

There exists a linear relationship between  $t_c$  and  $1/\kappa$  which can be expressed as

$$t_c = \left(\frac{\omega^2}{4}\right) \frac{1}{\kappa} \quad (39)$$

Here  $t_c$  and  $1/\kappa$  are the dependent and independent variables, and  $\omega^2/4$  is the slope and another one of the system constants. Recall that  $\omega$  is the beam radius at the cell. A least squares fit of a straight line to the  $t_c$  vs  $1/\kappa$  data gave  $\omega^2/4 = (8.62 \pm 0.1) \times 10^{-5} \text{ cm}^2$  as compared with the expected value of  $\omega^2/4 = (9.55 \pm 0.2) \times 10^{-5} \text{ cm}^2$  obtained by using  $z_1 = z_c\sqrt{3}$  and  $\omega_0^2 = (9.54 \pm 1.93) \times 10^{-5} \text{ cm}^2$  in Eq. (24).

The thermal lens equations developed here, Eqs. (34), (35), and (36), are based on the diffraction theory of aberrations and the assumption that the absorbance  $b$  of the sample is small, the beam radius within the sample  $\omega$  is nearly constant, the detector is placed at the beam center in the far field so that  $z_2 \gg z_c$ , and the  $\theta$  parameter is 0.12 or less as suggested by Fig. 8. Fits of the equations to data taken on samples with known properties yielded values for the system constants  $z_c$ ,  $0.24Pl/\lambda$ , and  $\omega^2/4$  that were within 10% of their expected values. These results support the validity of the equations and establish their usefulness.

Reproducibility in  $\theta$  was excellent, but in  $t_c$  it was often rather poor. As mentioned, factors involved in this seemed to have been lateral cell positioning, beam centering, and spatial noise on the beam. The spatial noise appears to have been the major source of error. Nevertheless, when fits of Eq. (36) to data were very good, both  $\theta$  and  $t_c$  were quite reproducible and very close to their expected values.

Since the equations are based on the aberrant nature of the thermal lens, they are able to make quantitative predictions that are more accurate than predictions made by the equations based on the parabolic or thin lens approximation. Thus the thermal lens technique is an accurate as well as a simple means of measuring the thermo-optic properties of weakly absorbing materials.

## References

1. J. P. Gordon, R. C. C. Leite, R. S. Moore, S. P. S. Porto, and J. R. Whinnery, *J. Appl. Phys.* **36**, 3 (1965).
2. J. R. Whinnery, *Acc. Chem. Res.* **7**, 225 (1974).
3. C. Hu and J. R. Whinnery, *Appl. Opt.* **12**, 72 (1973).
4. R. Dennemeyer, *Introduction to Partial Differential Equations and Boundary Value Problems* (McGraw-Hill, New York, 1968), pp. 294–295.
5. A. E. Siegman, *Introduction to Lasers and Masers* (McGraw-Hill, New York, 1971), pp. 305–307.
6. M. Abramowitz and I. A. Stegun, Eds., *Handbook of Mathematical Functions* (Dover, New York, 1972), pp. 228–229.
7. M. Born and E. Wolf, *Principles of Optics* (Pergamon, New York, 1965), pp. 459–464.
8. A. Yariv, *Introduction to Optical Electronics* (Holt, Rinehart & Winston, New York, 1971), p. 67.
9. R. E. Weast, Ed., *CRC Handbook of Chemistry and Physics* (CRC Press, Cleveland, 1977).
10. D. Solimini, *J. Appl. Phys.* **37**, 3314 (1966).

Meetings Calendar continued from page 1633

29–7 July CIE 20th Session, Warsaw U.S. Nat. Comm., CIE, c/o NBS, Wash., D.C. 20034

## August

28–2 Sept. 186th ACS Natl. Mtg., Wash., D.C. A. T. Winstead, 1155 16th St. N.W., Wash., D.C. 20036

## September

5–9 1983 Fourier Transform Spectroscopy Int. Conf., Durham J. Birch, Div. Electrical Science, National Physical Lab., Teddington, Middlesex, England

6–9 2nd Int. Conf. on Lasers, Beijing C. P. Wang, P.O. Box 92957, Los Angeles, Calif. 90009

## October

17–21 OSA Annual Mtg., New Orleans OSA, Mtgs. Dept., 1816 Jefferson Pl., Wash., D.C. 20036

23–26 9th European Conf. on Optical Communication, Geneva W. Steffen, Technical Centre PTT, 3000 Bern 29, Switzerland

## November

7–11 APS Div. of Plasma Physics, Seattle W. W. Havens, Jr., 335 E. 45 St., N. Y., N.Y. 10017

1984

? Optical Interference Coatings, 3rd OSA Topical Mtg. OSA, Mtgs. Dept., 1816 Jefferson Pl., Wash., D.C. 20036

? ICO 1984 General Assembly, Japan H. Gamo, 3812 Inlet Isle Dr., Corona del Mar, Calif. 92625

## January

23–25 Optical Fiber Communication, OSA Top. Mtg., New Orleans OSA, Mtgs. Dept., 1816 Jefferson Pl., Wash., D.C. 20036

## April

8–13 187th ACS Natl. Mtg., St. Louis A. T. Winstead, 1155 16th St. N.W., Wash., D.C. 20036

10–12 OSA Conf. on Lasers & Electro-Optics, Anaheim OSA, Mtgs. Dept., 1816 Jefferson Pl., Wash., D.C. 20036

## August

20–24 ICO-13, Sapporo, Japan S. Ballard, U. Florida, Physics Dept., 215 Williamson Hall, Gainesville, Fla. 32611